Anti-Ca^{2+} channel antibody attenuates Ca^{2+} currents and mimics cerebellar ataxia *in vivo*

Yaping Joyce Liao*†‡, Parsa Safa*, Yi-Ren Chen*, Raymond A. Sobel§, Edward S. Boyden*, and Richard W. Tsien*‡

Departments of *Molecular and Cellular Physiology, †Ophthalmology and Neurology, and §Pathology, Stanford University School of Medicine, Stanford, CA 94305

Voltage-gated Ca^{2+} channels (VGCCs) are membrane proteins that determine the activity and survival of neurons, and mutations in the P/Q-type VGCCs are known to cause cerebellar ataxia. VGCC dysfunction may also underlie acquired peripheral and central nervous system diseases associated with small-cell lung cancer, including Lambert–Eaton myasthenic syndrome (LEMS) and paraneoplastic cerebellar ataxia (PCA). The pathogenic role of anti-VGCC antibody in LEMS is well established. Although anti-VGCC antibody is also found in a significant fraction of PCA patients, its contribution to PCA is unclear. Using a polyclonal peptide antibody against a major immunogenic region in P/Q-type VGCCs (the extracellular Domain-III S5–S6 loop), we demonstrated that such antibody was sufficient to inhibit VGCC function in neuronal and recombinant VGCCs, alter cerebellar synaptic transmission, and confer the phenotype of cerebellar ataxia. Our data support the hypothesis that anti-VGCC antibody may play a significant role in the pathogenesis of cerebellar dysfunction in PCA.

Lambert–Eaton myasthenic syndrome | paraneoplastic | P/Q-type | N-type | neurotransmission

The association between anti-voltage-gated Ca^{2+} channel (VGCC) antibody and paraneoplastic cerebellar ataxia (PCA) dates back several decades to clinical observations of the coexistence of small-cell lung cancer with either cerebellar ataxia, Lambert–Eaton myasthenic syndrome (LEMS), or both (1, 2). The majority of these cancer patients with neurological symptoms have antibody against different types of VGCCs, especially P/Q- and N-type (3–5). The presence of different antibodies may be the consequence of an autoimmune response against the cancer cells (6, 7), known to express different VGCCs (8). There is conclusive evidence that the peripheral disease LEMS is caused by anti-VGCC antibodies, which diminish the availability of P/Q-type channels of the motor nerve terminals (9, 10).

In contrast, much less is known about the origin of cerebellar ataxia associated with anti-VGCC antibody, although VGCCs are prominent in cerebellar neurons (11, 12), and mutations in the P/Q-type VGCC cause ataxia (13). PCA patients have a high titer of anti-VGCC antibody (14–17) and undergo a selective loss of P/Q-type VGCC-containing cerebellar neurons (2, 18). Sera from LEMS patients, known to contain anti-VGCC antibodies, reduce P/Q-type VGCC surface expression in cerebellar granule and Purkinje neurons (19), consistent with an overlap of clinical syndromes between LEMS and PCA and, possibly, of pathogenic mechanism. There is no evidence to date that passive transfer of sera from LEMS or PCA patients is sufficient to cause central nervous system disease. Based on epitope mapping of antibody repertoire in patients with paraneoplastic neurological syndromes and small-cell lung cancer, we generated an antibody against a major epitope in the P/Q-type VGCC and evaluated its ability to affect cerebellar VGCC function and motor behavior.

Results

Functional Effects of Anti-VGCC Antibody. We looked for a functional effect of the Domain-III S5–S6 loop (D-III) antibody by using whole-cell voltage-clamp recordings of cerebellar granule cells, known to express N-, P/Q-, L-, and R-type VGCCs (20). The D-III serum (1:100 dilution) inhibited the Ca^{2+} current rapidly and reversibly (Fig. 1B). The sensitivity of the Ca^{2+} current to ω-conotoxin-GVIA (GVIA) and ω-agatoxin-IVA (ω-Aga-IVA) demonstrated the presence of N- and P/Q-type VGCCs, respectively, in the same neuron (Fig. 1B). After inhibition of both N- and P/Q-type VGCCs, the D-III serum had no further effect, indicating that it spared non-N- and P/Q-type Ca^{2+} currents. Preblock by ω-Aga-IVA did not abolish antibody inhibition of Ca^{2+} currents (Fig. 1D); thus, the D-III antibody did not inhibit solely P/Q-type VGCCs. Preblock with GVIA indicated that the D-III antibody did not selectively inhibit N-type VGCCs (data not shown). Taken together, these data suggest that the D-III antibody inhibited both N- and P/Q-type VGCCs.

Interestingly, the converse experiment, preblock by the D-III serum followed by toxin, led to an occlusion of the GVIA effect (Fig. 1 D–F), consistent with a competition between the D-III antibody and GVIA for N-type VGCCs. These results would make sense if antibody and GVIA both bound near the permeation pathway. However, the presence of D-III antibody did not abolish inhibition by ω-Aga-IVA (Fig. 1 E and F), known to affect channel gating by binding to a site other than the pore (21).

Antibody Inhibition of Heterologously Expressed Ca^{2+} Channels. Having obtained these tantalizing results in cerebellar granule neurons, we set out to study the mechanism of antibody action more specifically. We purified the IgG fraction of the rabbit serum and assessed its effects on human embryonic kidney (HEK293) cells expressing only one type of VGCC (Fig. 2A). The D-III IgG inhibited N-type Ca^{2+} current most significantly, reaching 41.0 ± 0.9% inhibition at 3 mg/ml (IC$_{50}$ = 115 μg/ml) (Fig. 2B), whereas control IgG had no effect (data not shown). D-III IgG also inhibited P/Q-type VGCCs, although less effectively (20.1 ± 2.6% inhibition at 3 mg/ml, IC$_{50}$ = 245 μg/ml). D-III IgG had no effect on L-type Ca^{2+} current at 3 mg/ml.

Because the D-III epitope is located near the GVIA-binding site, we looked further for possible competition between the D-III antibody and GVIA. Indeed, in HEK293 cells expressing N-type VGCCs, GVIA was significantly less effective in the presence of D-III IgG (Fig. 2C); the time constant (τ) of current reduction was 534 ± 124 s, a 10-fold increase over that found with GVIA alone (τ = 51.5 ± 3.8 s). There was no competition between D-III IgG (1 or 3 mg/ml) and ω-Aga-IVA (500 nM) in HEK293 cells expressing P/Q-type VGCCs (data not shown). The competition between the D-III IgG and GVIA but not ω-Aga-IVA provided further evidence that the D-III antibody

NEUROSCIENCE
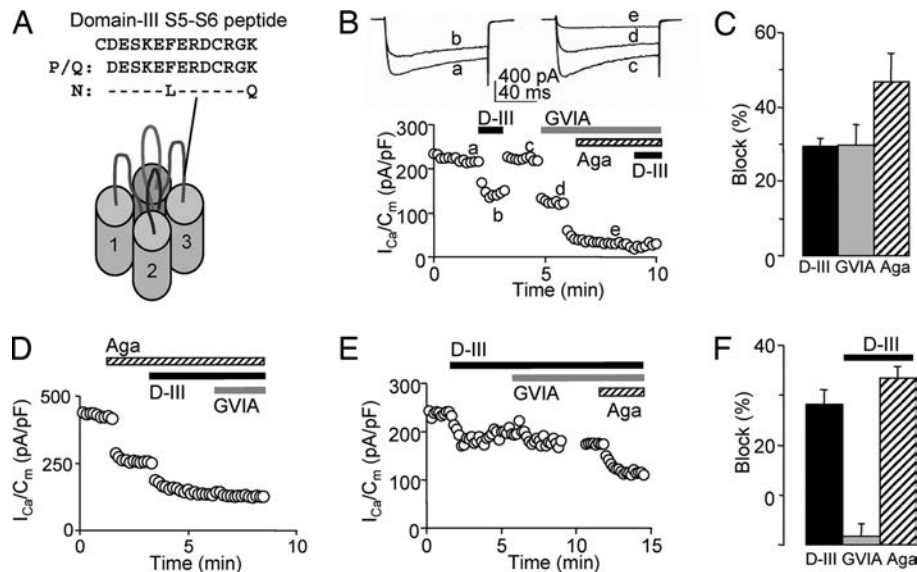
Fig. 1. Antibody against the extracellular D-III S5–S6 loop inhibited Ca^{2+} current in cultured cerebellar granule cells. (*A*) Amino acid sequence of the D-III peptide, which is 100% identical to P/Q-type and 85% identical to N-type VGCCs, typical of the high homology these channels share (41). (*B*) D-III serum decreased peak Ca^{2+} current density in a cerebellar granule cell with N-type (blocked by GVIA) and P/Q-type [inhibited by ω-Aga-IVA (Aga)] VGCC. The traces labeled a–e correspond to the data points shown below. (*C*) Pooled data showing block by D-III serum ($29.5 \pm 2.2\%$, $P < 0.0001$, $n = 21$), GVIA ($29.6 \pm 5.8\%$, $P < 0.001$, $n = 4$), and ω-Aga-IVA ($46.8 \pm 7.8\%$ inhibition, $P < 0.02$, $n = 3$). (*D*) After preblock by ω-Aga-IVA (41% inhibition), D-III serum reduced total Ca^{2+} current density by 26% and occluded further block by GVIA. (*E*) Preblock by the D-III serum occluded GVIA but not ω-Aga-IVA inhibition. (*F*) Summary of occlusion experiments. Preblock by D-III serum ($29.0 \pm 1.7\%$ inhibition, $n = 7$) resulted in little further inhibition by GVIA ($1.7 \pm 2.8\%$, $n = 7$) but allowed substantial further inhibition by ω-Aga-IVA ($34.8 \pm 2.3\%$, $n = 6$). D-III serum was at 1:100 dilution; GVIA, 2 μM; ω-Aga-IVA, 500 nM. (*C* and *F*) Error bars are SEM.

exerted inhibitory effects on VGCCs by interacting with residues near the channel pore. Overall, the findings in HEK cells were entirely consistent with the data in the cerebellar granule neurons.

Inhibition of VGCC in Presynaptic Terminals. With the useful precedent of LEMS in mind, we wanted to know whether at central synapses, as at the neuromuscular junction, anti-VGCC antibody affects presynaptic function. At the synaptic output of the cerebellar granule axons, the parallel fiber–Purkinje cell synapse, presynaptic P/Q- and N-type VGCCs are the main regulators of neurotransmitter release (12). Excitatory postsynaptic currents (EPSCs), recorded in the Purkinje cell soma under whole-cell voltage-clamp, were rapidly inhibited by the D-III IgG (100 μg/ml) to $52.2 \pm 7.2\%$ of baseline (Fig. 3), without a significant change in the access resistance or leak. IgG exposure also resulted in an increase in the facilitation of synaptic transmission during high-frequency repetitive stimulation (Fig. 3*D*). These IgG experiments confirmed our early studies with diluted rabbit serum (data not shown). Whereas the D-III serum inhibited EPSCs, synaptic transmission was not altered by the serum from another rabbit immunized with a Domain-IV S5–S6 (D-IV) peptide (22, 23). These results indicated that the D-III antibody lowered presynaptic release probability, an effect that could be counteracted by the accrual of effects of activity-dependent Ca^{2+} entry upon high-frequency stimulation.

Antibody Infusion over the Cerebellum Led to Ataxia. To look for an *in vivo* effect of the D-III antibody on motor behavior, we slowly infused D-III IgG (4–6 mg) into the subarachnoid fluid space over the mouse cerebellum. The surgery and behavioral assessments were done in a blinded fashion, with nonspecific rabbit IgG as a control. The similar and relatively selective delivery of rabbit IgG over the entire cerebellum was confirmed (Fig. 4*B*). Motor impairment was apparent in mice throughout the 3 days of D-III IgG infusion; they performed 30% less well on the

accelerated Rota Rod test than controls ($P \leq 0.04$, repetitive ANOVA; $n = 7$ each) (Fig. 4*C*). We also tested mice infused with D-IV IgG. In contrast to the D-III mice, mice exposed to the D-IV IgG performed as well as control mice ($P < 0.4$, repetitive ANOVA; D-IV IgG-infused mice, $n = 6$; control IgG-infused mice, $n = 9$).

To ascertain the cause of the poor motor performance by the D-III mice, we digitally analyzed the mouse gait during the Rota Rod test. Compared with control mice, the D-III mice exhibited a distinctively irregular gait pattern (Fig. 4*D*), often with visibly widened interhind paw distance. In this abnormal gait, the D-III mice took more steps to stay on the rod (Fig. 4*E*) and were more likely to take short steps or skips, defined as step duration lasting ≤ 0.5 s (Fig. 4*F*). The skips often occurred in series and sometimes in a direction that facilitated falling. This gait could not be attributed to decreased locomotive drive (Fig. 4*G*) or to weakness (Fig. 4*H*). However, the overall pattern of irregular gait and poor motor planning was strikingly similar to the abnormal motor behavior observed in PCA patients.

Histological study at the end of infusion revealed no evidence of neuronal loss, cell death, or inflammation in D-III or control IgG-infused mice by TUNEL stain (Fig. 4 *I* and *K*) or by transmission electron microscopy (Fig. 4 *J* and *L*). This result indicates that neurodegeneration is not responsible for the significant gait abnormality in the D-III mice.

Discussion

Here, we have described the pathogenic actions of a functional peptide antibody, designed to target a disease-relevant, biophysically critical portion of the P/Q- and N-type VGCCs. We showed that antibody against the D-III region specifically inhibited somatic VGCCs in transfected HEK293 cells and cerebellar granule neurons and impaired synaptic transmission in the acute cerebellar slice by its action on presynaptic VGCCs. This inhibition of synaptic transmission could have occurred by a reduction in single channel current, channel number, or both. The
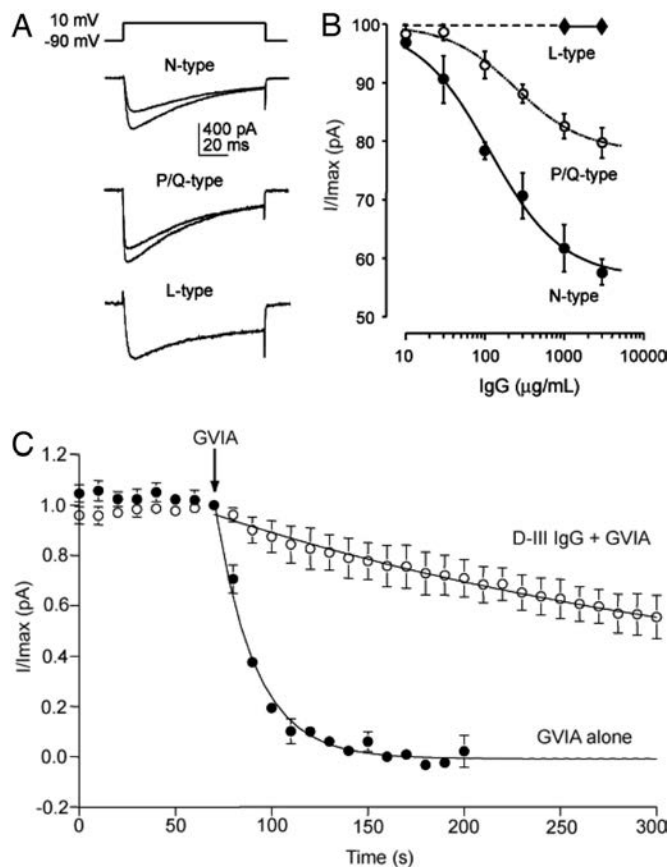
Fig. 2. Purified D-III IgG inhibited Ca²⁺ current in HEK293 cells expressing N-, P/Q-, or L-type VGCCs. (*A*) N-, P/Q-, and L-type Ca²⁺ current before (*Bottom* traces) and after (*Top* traces) exposure to 100 μg/ml D-III IgG. The before and after traces for the L-type Ca²⁺ currents coincide because D-III IgG had no effect. (*B*) D-III IgG dose–response graph for N-, P/Q-, and L-type channels. $n \geq 3$ per determination. (*C*) Preblock by D-III IgG partially occluded the GVIA inhibition of N-type Ca²⁺ current, with a 10-fold increase in the time constant (τ) of current reduction. D-III IgG + GVIA, $\tau = 534 \pm 124$ s vs. GVIA alone, $\tau = 51.5 \pm 3.8$ s, calculated based on a curve fit by a single exponential. $n = 3$ each. D-III IgG concentration was 1,000 μg/ml; GVIA, 4 μM. (*B* and *C*) Error bars are SEM.

Fig. 3. D-III IgG decreased glutamatergic synaptic transmission and altered short-term plasticity at the parallel fiber–Purkinje cell synapse in acute cerebellar slices. (*A*) Excitatory postsynaptic current before (a) and during (b) continuous D-III IgG (100 μg/ml) perfusion. (*B*) Rapid effect of the D-III IgG on the EPSC. (*C*) Representative EPSC during 40-Hz high-frequency repetitive stimulation before (*Upper*) and during (*Lower*) D-III IgG perfusion. (*D*) Pooled EPSC and facilitation before (○), during D-III IgG perfusion (▲), and after wash for >15 min (□). During D-III IgG exposure, $EPSC_1$ was reduced to $53.0 \pm 16.1\%$ of control ($P < 0.001$, $n = 4$), whereas $EPSC_{10}$ decreased to $75.5 \pm 10.7\%$. Facilitation, calculated as $100\% \times (EPSC_{8-10}/EPSC_1)$, increased from $281 \pm 21\%$ at baseline to $514 \pm 133\%$ during D-III IgG exposure ($P < 0.002$, $n = 4$). Error bars are SEM.

ability of the D-III antibody to slow the onset of action of GVIA by 10-fold is particularly notable because GVIA also binds to residues in the D-III region, the same region that encompasses the antibody epitope. Together, these findings strongly imply that the D-III antibody, like GVIA, binds near the channel pore. To look for effects of antibody *in vivo*, simulating what may happen in human disease, the D-III antibody was infused over the cerebellum, therefore bypassing the blood–brain barrier and avoiding the potential confounding behavioral effects of anti-VGCC antibody at the neuromuscular junction. Mice infused with D-III antibody exhibited cerebellar ataxia, characterized by irregular and excessive steps and skips. This altered motor behavior was observed in the absence of inflammation or neurodegeneration, consistent with a disease model where an antibody-mediated disruption of neurophysiology plays a major role in the pathogenesis of neurological symptoms.

We describe here a successful passive transfer model of a central nervous system channelopathy generated by anti-VGCC antibody, and we strongly support the significant role of antibody in the pathogenesis of PCA. Our work is complementary to human IgG passive-transfer models, both of LEMS (24, 25) and of cerebellar ataxia associated with antibody against metabotropic glutamate receptors (26). Our work establishes the central

pathogenicity of antibody against the D-III region. The high homology between P/Q- and N-type VGCCs in this region supports one explanation for the ability of sera from LEMS patients to inhibit more than one type of high-voltage-activated Ca²⁺ channels: the antibodies target a well conserved epitope (27). In contrast, antibody against D-IV (22, 23), another epitope commonly found in LEMS patients (28), neither reduced Ca²⁺ influx into parallel fiber terminals in cerebellar slices nor caused loss of motor ability *in vivo*. Our results were consistent with the finding that the D-IV antibody failed to bind to intact cells derived from small-cell lung cancer, but only to solubilized cells (23). This pattern of domain-specific pathogenicity parallels findings in animal models of LEMS, where immunization with a D-III but not a D-IV peptide successfully replicates the peripheral disease (23, 29).

Our data highlight the importance of the D-III region, an epitope common to both N- and P/Q-type VGCCs. Historically, the first antibody associated with LEMS and PCA is against VGCC labeled by GVIA (N-type channel) (30, 31), although antibody against uniquely N-type epitopes is not likely to contribute to the pathogenesis of LEMS because of the predominance of P/Q-type VGCCs after development of the neuromuscular junction is completed (32). Because the N- and P/Q-type VGCCs are both present and important for synaptic transmission in the central nervous system (12, 33, 34), antibodies against

NEUROSCIENCE

Fig. 4. Mice with brain infusion of D-III IgG exhibited cerebellar ataxia in the absence of neurodegeneration. (*A*) Mouse brain after infusion of a test dye, Fast green, over the cerebellum. Red arrow, site of cannula implantation; CTx, cerebral cortex; CB, cerebellum. (*B*) Montage of a coronal section of the postinfusion cerebellum stained with goat anti-rabbit IgG (green). BS, brainstem; 4th vent, fourth ventricle. (*C–H*) Blue, control IgG-infused mice; red, D-III IgG-infused mice. $n = 7$ unless otherwise stated. (*C*) Motor performance on the accelerated Rota Rod in nine trials performed over 3 days of IgG infusion. Longer fall latency corresponds to superior motor ability. The D-III mice performed 30% less well on the accelerated Rota Rod test than control mice ($P < 0.04$, repetitive ANOVA). (*D*) Representative 10-s digitized mouse gait during the Rota Rod test for a control mouse (*Upper*) and a D-III mouse (*Lower*). Each circle denotes the position of a hind paw, starting at 21 s into the Rota Rod test and ending with a fall for the D-III mouse 10 s later. The control mouse stayed on the rod for another 90 s (data not shown). Because the rod rotates downward, the hind paw position gradually decreased with respect to time as the mice stood on the rod. Open circles denote the paw position right after the mouse took a step. (*E*) Number of steps per min on the Rota Rod. D-III, 70 ± 4 steps per min vs. control, 53 ± 3 steps per min; *, $P < 0.02$. (*F*) Number of skips per min on the Rota Rod. D-III, 13.3 ± 2.9 skips per min vs. control, 1.7 ± 0.9 skips per min; **, $P = 0.002$. (*G*) Percentage time spent ambulating in open field. D-III, $34 \pm 5\%$ vs. control, $36 \pm 6\%$, two trials per mouse. $P = 0.75$. (*H*) Frequency of vertical stance (free standing on fully extended hind limbs). D-III, 1.5 ± 0.4 times per min vs. control, 1.3 ± 0.3 times per min, two trials per mouse; $P = 0.71$. (*C* and *E–H*) Error bars are SEM. (*I* and *K*) Absence of TUNEL staining for dying neurons in the cerebellar cortex from control mice ($n = 4$) (*I*) and D-III mice ($n = 3$) (*K*). (*J* and *L*) Transmission electron microscopy shows normal morphology of Purkinje cells from the cerebellum of control (*J*) and D-III (*L*) mice. $n \geq 3$; mol, molecular layer; Pur, Purkinje cell layer; gr, granule cell layer; nuc, nucleus; cyto, cytoplasm. [Scale bars: 25 μm (*I* and *K*); 0.25 μm (*J* and *L*).]

epitopes that are uniquely specific to N-type or P/Q-type or shared by both VGCCs may contribute to PCA. This last possibility is highly likely given the significant degree of homology between the pore-forming subunit of N- and P/Q-type VGCCs. In the particular case of the D-III epitope, which is 85% identical between the two channel types, antibody block of N-type channels was at least as great as that of P/Q-type channels. Given the presence of antibodies against both kinds of VGCCs in the cerebrospinal fluid of PCA patients (16, 17), it seems likely that reductions in both N- and P/Q-type Ca^{2+} entry may contribute to the observed motor behavior.

Interestingly, the actions of the D-III antibody on N- and P/Q-type channels were reminiscent of the effects of the spider toxin ω-Aga-IIIA (35, 36). Like D-III antibody, ω-Aga-IIIA caused only partial block of N-type channels even at maximal effective doses, but it rendered the remaining N-type current impervious to further blockade by GVIA (21, 35), as if it had occupied part of the GVIA-binding site. In a further parallel, both D-III antibody and ω-Aga-IIIA caused only partial inhibition of P/Q-type channels at saturating concentrations but failed to prevent further reduction of current by ω-Aga-IVA, a gating modifier (21, 35). Nothing is published about the structural basis of ω-Aga-IIIA binding, but one can be reasonably confident that D-III antibody interacts with the S5–S6 region of Domain-III, in close proximity to structural determinants of GVIA binding (37, 38). Furthermore, we found that binding of D-III antibody slows the on-rate for GVIA, as expected for direct competition, rather than an antagonistic allosteric action merely involving speeding of inhibitor off-rate. Taken together, the evidence lends strong support to a scenario whereby the partial inhibitor (in this case D-III antibody) occupies a structural determinant important for GVIA (the S5–S6 loop) and thus opposes toxin binding.

Our description of the pathophysiological effects of the D-III antibody as a direct inhibitory agent is not mutually exclusive with disease mechanisms involving channel down-regulation. IgG from LEMS patients produces antibody cross-linking of adjacent VGCCs, internalization of the antibody-VGCC complex, and reduction of channel surface expression (9, 10). Alterations in cerebellar physiology by some combination of functional inhibition and channel down-regulation can explain the disturbance of cerebellar circuitry and profound neurological symptoms early in the disease, before overt anatomical changes appear. Our work suggests that a reduction of disease-causing antibodies in the early stage of disease might be a useful therapeutic intervention, not only as a means of forestalling later neurodegeneration but also as a strategy to restore normal channel function and neurophysiology.

Materials and Methods

Antibody Generation. We raised rabbit polyclonal antibodies against the D-III or the D-IV S5–S6 loops of the mouse α_{1A} subunit of P/Q-type VGCCs, which contain major immunogenic epitopes found in significant percentages of patients with anti-VGCC antibody (22, 23, 39). The D-III peptide also shares 85% sequence identity to the corresponding region in the N-type VGCCs (Fig. 1A). This extracellular loop is a biophysically important part of the channel: it is located near the channel pore, the binding site for the N-type VGCC blocker GVIA (37, 38), and a putative Ca^{2+}-binding site important for Ca^{2+} channel permeation (40). The peptides (D-III, DESKEFERDCRGK; D-IV, IDGEDEDSD-EDEF) were synthesized at the Stanford Protein and Nucleic Acid Facility, conjugated to keyhole limpet hemocyanin, and injected into rabbits by Animal Pharm Services, Inc. Rabbit IgGs were purified with Montage protein A columns (Millipore) and stored in PBS. Protein concentration was determined with the MicroBCA kit (Pierce), and the presence of purified IgG heavy and light chains was confirmed by gel electrophoresis.

Cell Cultures and Transfection. Dissociated cerebellar granule cells were prepared from P4-P8 mouse cerebella and grown in culture as described in ref. 20. The cells were maintained in MEM (Invitrogen), 10% FBS, 5 mg/liter glucose, 100 mg/liter transferrin, 25 mg/liter insulin, and 300 mg/liter glutamine. Cells were plated on Matrigel (Collaborative Biomedical Products)-coated glass

coverslips. HEK293 cells, stably expressing the α_2-δ and β_{1C} VGCC subunits, were grown in DMEM (Invitrogen), 10% FCS, 100 units/ml penicillin, 100 μg/ml streptomycin, and 400 μg/ml Geneticin, and transiently transfected with cDNAs encoding either the α_{1A} (a gift from G. Zamponi, University of Calgary, Calgary, AB, Canada), α_{1B}, or α_{1C} subunit, and the GFP by using the Lipofectamine 2000 reagent (Invitrogen). All cells were maintained in a humidified, 37°C incubator with 95% O_2/5% CO_2.

Electrophysiology. A conventional whole-cell patch-clamp technique was used to record Ca^{2+} channel activity in cerebellar granule cells or transfected HEK293 cells. Glass electrodes (2.5–3.5 MΩ) contained an internal solution of 109 mM CsCl, 4.5 mM MgCl$_2$, 1 mM EGTA, 4 mM ATP, 0.3 mM GTP, 25 mM Hepes, 10 mM phosphocreatine, and 20 units/ml creatine phosphokinase, pH 7.3; 295 mOsm was used to establish GΩ seals, while cells were in 119 mM NaCl, 5 mM KCl, 2 mM CaCl$_2$, 1 mM MgCl$_2$, 30 mM glucose, and 25 mM Hepes, pH 7.3, 305 mOsm. Recordings were performed in an external solution containing 155 mM triethylammonium chloride, 10 mM CaCl$_2$, 10 mM Hepes, and 10 mM glucose, pH 7.3, 305 mOsm, with step depolarization from the holding potential of -90 to -10 to 20 mV for 80 ms at 10-s intervals (pClamp8; Molecular Devices and EPC7 amplifier; HEKA Electronic). Currents were low-pass-filtered at 3 kHz and digitized (Digidata; Molecular Devices) at 10 kHz. The recording chamber was not continuously perfused except during wash. Antibody or toxins were pipetted directly into the static chamber. All chemical and drugs were purchased from Sigma except for GVIA and ω-Aga-IVA (Peptide International).

For synaptic studies, 300-μm parasagittal acute cerebellar slices from 8- to 12-week-old C57BL/6 mice (Charles River) were prepared with a Vibratome (Leica) in cutting solution consisted of 175 mM sucrose, 20 mM NaCl, 3 mM KCl, 1.25 mM NaH$_2$PO$_4$, 26 mM NaHCO$_3$, 10 mM glucose, 2.4 mM CaCl$_2$, 1.3 mM MgCl$_2$, pH 7.3, 310 mOsm. The slices were allowed to recover for at least 1 hour in oxygenated artificial cerebrospinal fluid containing 124 mM NaCl, 3 mM KCl, 1.25 mM NaH$_2$PO$_4$, 26 mM NaHCO$_3$, 10 mM glucose, 2.4 mM CaCl$_2$, 1.3 mM MgCl$_2$, pH 7.3, 310 mOsm before recording in the presence of 10 μM gabazine (Tocris) to block inhibitory transmission. Glass electrodes (1.2–2.0 MΩ) containing internal solution with 150 mM cesium methanesulfonate, 8 mM NaCl, 0.1 mM CaCl$_2$, 0.6 mM MgCl$_2$, 1 mM EGTA, 4 mM Mg-ATP, 0.4 mM Na-GTP, 0.1 mM D600, and 2 mM QX314, pH 7.25, 305 mOsm were used to record from Purkinje cells in whole-cell configuration. Low-intensity stimulation was applied to the parallel fibers by a bipolar electrode (A.M.P.I. stimulator), while EPSCs were low-pass-filtered at 5 kHz and digitized at 10 kHz (Axopatch 1D amplifier, pClamp8; Digidata). Leak and access resistance were monitored continuously, and experiments were rejected if these parameters changed significantly. The data were analyzed with custom-written programs in IgorPro (WaveMetrics) and Microsoft Excel.

Brain Infusion. All animal care and handling were performed in accordance with guidelines of the Stanford Institutional Animal Care and Use Committee. All steps of surgery were performed by an investigator blinded to the identity of IgG infused. Ten-week-old male C57BL/6 mice (weight >20 g) were anesthetized with an i.p. injection of ketamine and meditomidine and placed in a stereotaxic apparatus (Kopf Instruments) with the body on top of a feedback-controlled heating pad to maintain core temperature at 37°C. Continuous isoflurane and oxygen were delivered nasally at 1–2 liter/min. Respiration, behavior, and body temperature of the mice were repeatedly assessed over the 5- to 10-min operative period. Each mouse had s.c. injections of lactated Ringer's solution to prevent dehydration and a single injection of atropine to reduce mucous secretion. The Alzet 30-g infusion cannula (custom tube length, 1.5 mm) was implanted into the subarachnoid space above the rostral, dorsal cerebellum, $\approx$3 mm caudal to lambda at midline. The Alzet osmotic pump (1003D, which delivers 1 μl/h over 3 days; Durect Corp.) was filled with control or experimental rabbit IgG (4–6 mg of IgG in 100 μl of PBS) and placed between the scapula. The amount of IgG infused was within the range of the Ca^{2+} channel IgG concentration found in the cerebral spinal fluid of patients with cerebellar ataxia associated with small-cell lung cancer (16). The cannula was secured with cyanoacrylate (VetBond; 3M) followed by dental cement (Hygenic), and the skin was closed with sutures. Intraperitoneal buprenorphine was given after surgery to reduce discomfort. Animals were monitored postoperatively until mobile, and at least twice daily. Multiple practice surgeries to infuse a low-molecular-weight dye Fast Green confirmed consistent delivery of the pump content (Fig. 4A). The delivery of rabbit IgG was confirmed after infusion with Alexa 488-labeled goat anti-rabbit IgG (Molecular Probes) staining of coronal sections through the cerebellum.

Behavioral Assessment. The behavioral experiments were carried out in an isolation room by an investigator blinded to the identity of infused IgG. Before surgery, the mice were habituated to the stationary Rota Rod once per day for 3 days, including the day of surgery, and once to the cage for open-field

locomotion. The mice were allowed to recover for ≈15 h after surgery, and their behavior was assessed once per day for 3 days. Each of the behavioral tests was administered at the same time of the day throughout. The accelerated Rota Rod (Economex; Columbus Instruments) was used to assess locomotive ability and learning, and three trials were done per day for 3 days (total of 9 trials) with a baseline speed of 4 rpm and acceleration of 0.1 rpm/s and 2–3 min of rest between trials in the same day. After the behavioral experiments were completed, video recordings of the Rota Rod performance of mice infused with D-III or control IgG were further analyzed with a digitizer (Silicon Coach). The videos (60 frames per s) were viewed frame by frame, and at least 30 s of the hind paw position on day 3 of infusion was manually digitized for each mouse to track changes over time. The steps per min and skips per min (defined as step duration ≤500 ms) were counted visually and confirmed by digitization for a trial on day 3. Each mouse was also observed and filmed in a blinded fashion in open-field locomotion for 5 min per day, and the amount of time the mouse was ambulatory in 2.5-min blocks and the number of times each mouse stood up independently with full extension of the hind limbs (vertical stance) was determined by visual inspection.

Histological Analysis. At day 3 after surgery, the mice were anesthetized with isoflurane and underwent intracardiac perfusion with PBS containing heparin, 4% paraformaldehyde, and 0.1% glutaraldehyde. Brains were sectioned in parasagittal and coronal planes, processed routinely, and embedded in paraffin. Four-micron sections were stained in H&E and analyzed in a blinded fashion by a trained neuropathologist. All mice had enlargement of the third, lateral, and fourth ventricles, consistent with a communicating hydrocephalus, likely secondary to the amount and rate of protein infused. Purkinje cell soma, dendrite, and axons were studied by anti-calbindin monoclonal antibody (Sigma) with routine immunohistochemical methods and visualized by Zeiss confocal microscopy. Because Purkinje and granule cell degeneration is known to occur in patients with paraneoplastic cerebellar ataxia, we looked for evidence of cell death in infused mice. We focused on the inferior vermis, a region far from the implantation site but well infused with IgG. The presence of fragmented DNA, a sign of apoptotic cell death, was assessed with a TUNEL kit (ApoTag; Oncor) with thyroid tissue as positive control. Slides were counterstained with hematoxylin and imaged with a Zeiss microscope with a 100× objective, NA 1.7, $n = 4$ for D-III mice and $n = 3$ for control mice. Evidence of any kind of cell death was also assessed by transmission electron microscopy. Coronal and parasagittal cerebellar sections from three experimental and three control mice were osmicated, serially dehydrated in ethanol, infiltrated with propylene oxide, and embedded in Epon epoxy resin. Thick sections were stained with toluidine blue and examined with a Zeiss light microscope to select an area in the caudal vermis for ultrathin sectioning. Eighty-nanometer sections were placed on carbon/Formvar-coated copper grids and stained with uranyl acetate and lead citrate, followed by viewing in a JEOL 1230 at 80 kV and photographed with a Gatan digital camera at 2–120,000×.

Statistical Analysis. A two-tailed Student's t test was used to determine the level of significance. Repetitive ANOVA was used to calculate the significance of the Rota Rod test.

1. Eaton LM, Lambert EH (1957) Electromyography and electric stimulation of nerves in diseases of motor unit: Observations on myasthenic syndrome associated with malignant tumors. *J Am Med Assoc* 163:1117–1124.
2. Satoyoshi E, Kowa H, Fukunaga N (1973) Subacute cerebellar degeneration and Eaton–Lambert syndrome with bronchogenic carcinoma: A case report. *Neurology* 23:764–768.
3. Pelucchi A, *et al*. (1993) Calcium channel autoantibodies in myasthenic syndrome and small-cell lung cancer. *Am Rev Respir Dis* 147:1229–1232.
4. Lennon VA, *et al*. (1995) Calcium channel antibodies in the Lambert–Eaton syndrome and other paraneoplastic syndromes. *N Engl J Med* 332:1467–1474.
5. Lang B, Newsom-Davis J (1995) Immunopathology of the Lambert–Eaton myasthenic syndrome. *Springer Semin Immunopathol* 17:3–15.
6. Darnell RB, Posner JB (2003) Paraneoplastic syndromes involving the nervous system. *N Engl J Med* 349:1543–1554.
7. Whitney KD, McNamara JO (1999) Autoimmunity and neurological disease: Antibody modulation of synaptic transmission. *Annu Rev Neurosci* 22:175–195.
8. Meriney SD, Hulsizer SC, Lennon VA, Grinnell AD (1996) Lambert–Eaton myasthenic syndrome immunoglobulins react with multiple types of calcium channels in small-cell lung carcinoma. *Ann Neurol* 40:739–749.
9. Vincent A, Lang B, Newsom-Davis J (1989) Autoimmunity to the voltage-gated calcium channel underlies the Lambert–Eaton myasthenic syndrome, a paraneoplastic disorder. *Trends Neurosci* 12:496–502.
10. Dalmau J, Gultekin HS, Posner JB (1999) Paraneoplastic neurologic syndromes: Pathogenesis and physiopathology. *Brain Pathol* 9:275–284.
11. Hillman D, *et al*. (1991) Localization of P-type calcium channels in the central nervous system. *Proc Natl Acad Sci USA* 88:7076–7080.
12. Mintz IM, Sabatini BL, Regehr WG (1995) Calcium control of transmitter release at a cerebellar synapse. *Neuron* 15:675–688.
13. Fletcher CF, Lennon VA (2003) Do calcium channel autoantibodies cause cerebellar ataxia with Lambert–Eaton syndrome? *Ann Neurol* 53:5–7.
14. Mason WP, *et al*. (1997) Small-cell lung cancer, paraneoplastic cerebellar degeneration, and the Lambert–Eaton myasthenic syndrome. *Brain* 120:1279–1300.
15. Wirtz PW, *et al*. (2005) P/Q-type calcium channel antibodies, Lambert–Eaton myasthenic syndrome, and survival in small-cell lung cancer. *J Neuroimmunol* 164:161–165.
16. Graus F, *et al*. (2002) P/Q type calcium channel antibodies in paraneoplastic cerebellar degeneration with lung cancer. *Neurology* 59:764–766.
17. Clouston PD, *et al*. (1992) Paraneoplastic cerebellar degeneration. III. Cerebellar degeneration, cancer, and the Lambert–Eaton myasthenic syndrome. *Neurology* 42:1944–1950.
18. Fukuda T, *et al*. (2003) Reduction of P/Q-type calcium channels in the postmortem cerebellum of paraneoplastic cerebellar degeneration with Lambert–Eaton myasthenic syndrome. *Ann Neurol* 53:21–28.
19. Pinto A, *et al*. (1998) Human autoantibodies specific for the α_{1A} calcium channel subunit reduce both P-type and Q-type calcium currents in cerebellar neurons. *Proc Natl Acad Sci USA* 95:8328–8333.
20. Randall A, Tsien RW (1995) Pharmacological dissection of multiple types of Ca^{2+} channel currents in rat cerebellar granule neurons. *J Neurosci* 15:2995–3012.
21. McDonough SI, Boland LM, Mintz IM, Bean BP (2002) Interactions among toxins that inhibit N-type and P-type calcium channels. *J Gen Physiol* 119:313–328.
22. Barry EL, Viglione MP, Kim YI, Froehner SC (1995) Expression and antibody inhibition of P-type calcium channels in human small-cell lung carcinoma cells. *J Neurosci* 15:274–283.
23. Black JL, *et al*. (1998) Lambert–Eaton myasthenic syndrome: Antigenicity of recombinant human P/Q-type calcium channel α_1 subunit putative ion pore region (domain IV, S5–S6). *Ann NY Acad Sci* 841:691–695.
24. Newsom-Davis J, *et al*. (1982) Lambert–Eaton myasthenic syndrome: Electrophysiological evidence for a humoral factor. *Muscle Nerve* 5:S17–S20.
25. Fukunaga H, Engel AG, Lang B, Newsom-Davis J, Vincent A (1983) Passive transfer of Lambert–Eaton myasthenic syndrome with IgG from man to mouse depletes the presynaptic membrane active zones. *Proc Natl Acad Sci USA* 80:7636–7640.
26. Sillevis Smitt P, *et al*. (2000) Paraneoplastic cerebellar ataxia due to autoantibodies against a glutamate receptor. *N Engl J Med* 342:21–27.
27. Garcia KD, Mynlieff M, Sanders DB, Beam KG, Walrond JP (1996) Lambert–Eaton sera reduce low-voltage and high-voltage activated Ca^{2+} currents in murine dorsal root ganglion neurons. *Proc Natl Acad Sci USA* 93:9264–9269.
28. Parsons KT, Kwok WW (2002) Linear B-cell epitopes in Lambert–Eaton myasthenic syndrome defined by cell-free synthetic peptide binding. *J Neuroimmunol* 126:190–195.
29. Komai K, Iwasa K, Takamori M (1999) Calcium channel peptide can cause an autoimmune-mediated model of Lambert–Eaton myasthenic syndrome in rats. *J Neurol Sci* 166:126–130.
30. Lennon VA, Lambert EH (1989) Autoantibodies bind solubilized calcium channel–ω-conotoxin complexes from small-cell lung carcinoma: A diagnostic aid for Lambert–Eaton myasthenic syndrome. *Mayo Clin Proc* 64:1498–1504.
31. Sher E, *et al*. (1989) Specificity of calcium channel autoantibodies in Lambert–Eaton myasthenic syndrome. *Lancet* 2:640–643.
32. Protti DA, Reisin R, Mackinley TA, Uchitel OD (1996) Calcium channel blockers and transmitter release at the normal human neuromuscular junction. *Neurology* 46:1391–1396.
33. Dunlap K, Luebke JI, Turner TJ (1995) Exocytotic Ca^{2+} channels in mammalian central neurons. *Trends Neurosci* 18:89–98.
34. Wheeler DB, Sather WA, Randall A, Tsien RW (1994) Distinctive properties of a neuronal calcium channel and its contribution to excitatory synaptic transmission in the central nervous system. *Adv Second Messenger Phosphoprotein Res* 29:155–171.
35. Mintz IM (1994) Block of calcium channels in rat central neurons by the spider toxin ω-Aga-IIIA. *J Neurosci* 14:2844–2853.
36. Mintz IM, Venema VJ, Adams ME, Bean BP (1991) Inhibition of N- and L-type Ca^{2+} channels by the spider venom toxin ω-Aga-IIIA. *Proc Natl Acad Sci USA* 88:6628–6631.
37. Ellinor PT, Zhang JF, Horne WA, Tsien RW (1994) Structural determinants of the blockade of N-type calcium channels by a peptide neurotoxin. *Nature* 372:272–275.
38. Feng ZP, *et al*. (2001) Residue Gly-1326 of the N-type calcium channel α_{1B} subunit controls reversibility of ω-conotoxin GVIA and MVIIA block. *J Biol Chem* 276:15728–15735.
39. Iwasa K, Takamori M, Komai K, Mori Y (2000) Recombinant calcium channel is recognized by Lambert–Eaton myasthenic syndrome antibodies. *Neurology* 54:757–759.
40. Feng ZP, *et al*. (2001) Amino acid residues outside of the pore region contribute to N-type calcium channel permeation. *J Biol Chem* 276:5726–5730.
41. Catterall WA (1998) Structure and function of neuronal Ca^{2+} channels and their role in neurotransmitter release. *Cell Calcium* 24:307–323.